Supporting Information

A "Three in one" strategy realized by fluorinated gold-doped titanium silicalite layer on copper current collector for stable lithium metal batteries

Xiaopan Jin[a], Gaoxu Huang[a], Xianming Zhao[a], Honghao Liu[a], Rongjie Wang[b,*], Mengjia Guan[a,*], Yongsheng Li[a,b,*]

[a] Lab of Low-Dimensional Materials Chemistry, Key Laboratory for Ultrafine Materials of Ministry of Education, Frontier Science Center of the Materials Biology and Dynamic Chemistry, Shanghai Engineering Research Center of Hierarchical Nanomaterials, School of Materials Science and Engineering, East China University of Science and Technology, Shanghai 200237, China.

[b] School of Chemistry and Chemical Engineering, State Key Laboratory Incubation Base for Green Processing of Chemical Engineering, Shihezi University, Shihezi 832003, China.

Corresponding authors: wangrongjie@shzu.edu.cn, guanmj@ecust.edu.cn, ysli@ecust.edu.cn

Experimental section

Materials

Tetraethyl orthosilicate (TEOS), tetrapropylammonium hydroxide (TPAOH), Tetrabutyl titanate (TBOT) and isopropanol (IPA) was purchased from Aladdin Reagent Co., Ltd. 3-Mercaptopropyltrimethoxysilane (MPTMS), chloroauric acid trihydrate ($HAuCl_4 \cdot 3H_2O$) and ammonium fluoride (NH_4F) were obtained from Macklin Reagent Co., Ltd. All chemicals were commercially available and used as received without further purification.

Synthesis of Au-doped titanium silicalite (ATS)

First 6.24 g TPAOH solution (25wt%) was dissolved in 16.5 g of deionized water, then 0.36 g MPTMS was slowly added and continuously stirred for 8h. Afterwards a certain amount of chlorauric acid aqueous was added into the above mixture and stirred for 1 h. After that, TEOS was added and stirred at 30 °C for 3h. The mixed solution was then transferred to a low temperature bath at 5 °C and 2.25g IPA containing 0.25g TBOT was added. After stirring for 12 h, the above solution was put into a 40 °C water bath and stirred for 2h. After cooling to room temperature, the slurry was transferred into a Teflon reactor and kept at 140 °C for 3 d. The product was collected by centrifugation and washed with deionized water for three times, dried at 100 ℃ for 10 h and calcined in air at 500 °C for 8 h to remove the organic templating agent. The synthesis of titanium silicalite (TS) is similar to that of ATS, except for the addition of chloroauric acid aqueous.

Synthesis of fluorinated Au-doped titanium silicalite (ATSF-x)

The fluoride modified ATS was prepared by impregnation method. The NH_4F solutions of various concentrations were added into the ATS powder. After ultrasonic treatment for 30 min, the obtained sample was rest at room temperature for 3 h, then dried at 110 °C overnight and calcined in air at 500 °C for 4 h. In terms of the concentration of NH_4F solution (wt%), the fluorinated ATS samples were denoted as ATSF-5, ATSF-15, ATSF-25, and ATSF-50 respectively.

Preparation of working electrodes

For the preparation of TS/Cu, ATS/Cu and ATSF-x/Cu electrodes, the active materials (TS, ATS and ATSF-x, x=5, 15, 25 and 50), carbon black and polyvinylidene difluoride

binder (PVDF) were added into in N-methyl-2-pyrrolidone (NMP) at a weight ratio of 7:2:1 to form a homogeneous slurry after being stirred 12h. The slurry was coated on a copper foil with a thickness of 50 μm and vacuum dried at 80 ℃ overnight. The electrode was punched into discs with a diameter of 12 mm.

The $LiFePO_4$ (LFP) cathode was made by mixing the commercial LFP powders, carbon black and polyvinylidene difluoride (PVDF) with a mass ratio of 8:1:1 with N-methyl-2-pyrrolidone as the solvent. The slurry was blade-coated on the aluminum foil and then dried at 60 ℃ for 12 h. The electrode was punched into discs with a diameter of 9 mm as the positive electrode. The areal mass loading of LFP was about 15.4 mg cm^{-2}.

Characterization

Field-emission scanning electron microscopy (FE-SEM, JEOL S-4800) combined with energy dispersive X-ray spectroscopy (EDS) and transmission electron microscope (TEM, JEM-2100) were adopted for characterizing micro-morphologies and microstructures. The crystal structures of all samples were determined by using X-ray powder diffraction (XRD) on a Bruker/D8 Focus diffractometer. Cu Kα radiation (λ=1.5405 Å) was generated at 40.0 kV and 40.0 mA, and reflections were recorded in the 2θ range from 2° to 50° with a scan rate of 6° min^{-1}. Fourier-transform infrared (FTIR) spectroscopy was performed with a FTIR spectrometer (Nicolet iS50) using KBr pellets to characterize the chemical structure of samples. The Brunauer–Emmett–Teller (BET) surface area and pore size distribution were measured based on the adsorption-desorption isotherm of nitrogen using a Micromeritics TriStar II 3020 analyzer. All the samples were degassed at 300 °C for 12 h under flowing N_2 before measurement. X-ray photoelectron spectroscopy (XPS) characterization was conducted on a Thermo ESCALAB 250 spectrometer to characterize the chemical composition and valence state of powder samples and the surface chemical composition of cycled electrodes.

Electrochemical measurements

Electrochemical performances were tested in the 2025-type coin cells. All the cells were assembled in the argon-filled glove box (oxygen and water content under 0.1ppm).

The electrolyte used in Li|Cu half cells and symmetric Li|Li cells was composed of 1 M bis(trifluoromethanesulfonyl)imide (LiTFSI) in 1,3-dioxolane/1,2-dimethoxyethane binary solvents (DOL/DME, v/v=1:1) with 2 wt% $LiNO_3$ as an additive. And the volume of the electrolyte in each Li|Cu half cell and symmetric Li|Li cell was 50 μL. To measure the Coulombic efficiency (CE), the ATSF-5/Cu and copper (Cu) foil were used as working electrodes, Celgard 2400 polypropylene as the separators and lithium metal as the as the counter electrodes. The cells were first cycled at 50 μA for 5 cycles from 0-1V to stabilize the interface then cycled with different current densities. For symmetric Li|Li cells, the cell was assembled with ATSF-5/Cu and copper (Cu) foil as the working electrode and Li foil as the counter electrode to deposit Li (6 mA h cm^{-2}) on the ATSF-5/Cu and Cu foil electrode at a current density of 0.5 mA cm^{-2}. Electrochemical impedance spectroscopy (EIS) and was performed on an electrochemical working station (Chenhua CHI 600) in the frequency range from 0.01 HZ to 100 kHZ. The assembled full cells of ATSF-5/Cu–Li||LFP and Cu–Li||LFP were measured in a potential range of 2.8–4.2 V. For the Li-LFP full cells, 50μL of 1.0 M $LiPF_6$ in ethylene carbonate/diethylcarbonate solution (EC/DEC, v:v=1:1) with 10% FEC was used. The galvanostatic charge-discharge test was carried out on battery test systems (CT2001C, LAND).

Computational method

The first-principles [S1, S2] was employed to perform all Spin-polarization density functional theory (DFT) calculations within the generalized gradient approximation (GGA) using the Perdew-Burke-Ernzerhof (PBE) [S3] formulation. The projected augmented wave (PAW) potentials [S4, S5] was chosen to describe the ionic cores and take valence electrons into account using a plane wave basis set with a kinetic energy cutoff of 520 eV. Van der Waals interactions have been considered using the DFT-D3 method of Grimme [S6, S7]. The electronic energy was considered self-consistent when the energy change was smaller than 10^{-5} eV. A geometry optimization was considered convergent when the energy change was smaller than 0.02 eV $Å^{-1}$. During the relaxation, the Brillouin zone with a 3 × 3 × 1 Gamma centered grid was used. The 15 Å vacuum layer

was normally added to the surface to eliminate the artificial interactions between periodic images. Spin polarized calculations were performed for this calculation.

The adsorption energy (E_{ads}) was defined as:

$$E_{ads} = E_{total} - E_{slab} - E_{Li}$$

where E_{total} is the total energy of Li dsorbed on the optimized slab, E_{slab} is the energy of pristine Au or Cu slab, and E_{Li} is the energy of an Li atom.

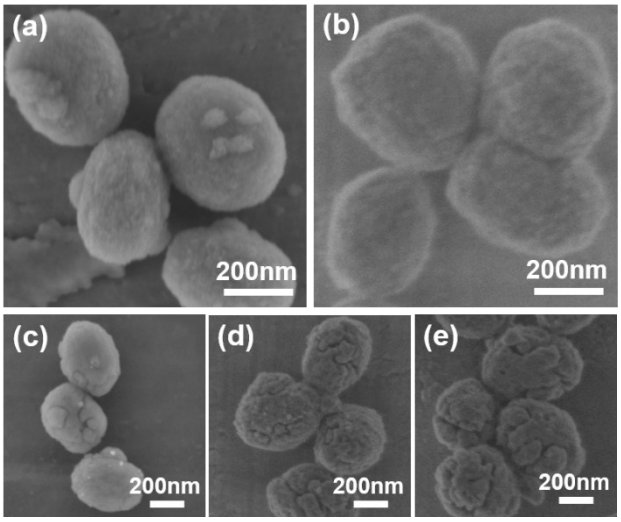

Figure S1. SEM images of (a) TS, (b) ATS and (e-g) fluorinated ATS at different NH_4F solution concentrations of 15 wt%, 25 wt% and 50 wt%.

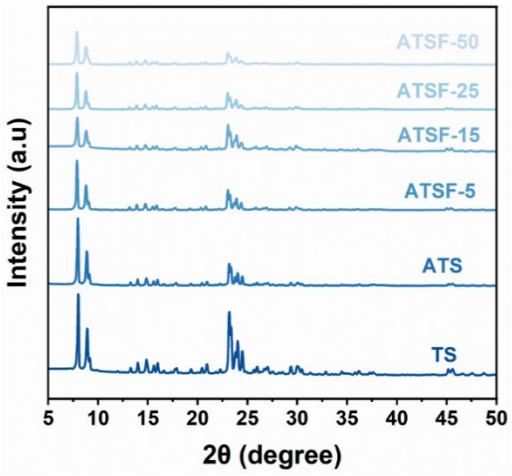

Figure S2. XRD patterns of TS, ATS and fluorinated ATS at different NH_4F solution concentrations of 5wt%, 15 wt%, 25 wt% and 50 wt%.

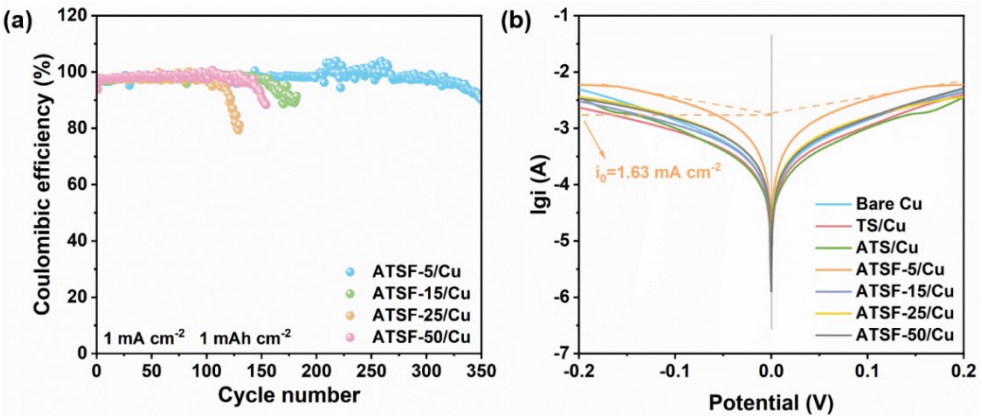

Figure S3. (a) CE comparison of ATSF-5/Cu, ATSF-15/Cu, ATSF-25/Cu and ATSF-50/Cu electrodes with capacity of 1 mAh·cm^{-2} at 1 mA·cm^{-2}. (b) Tafel curves of bare Cu, TS/Cu, ATS/Cu, ATSF-5/Cu, ATSF-15/Cu, ATSF-25/Cu and ATSF-50/Cu electrodes.

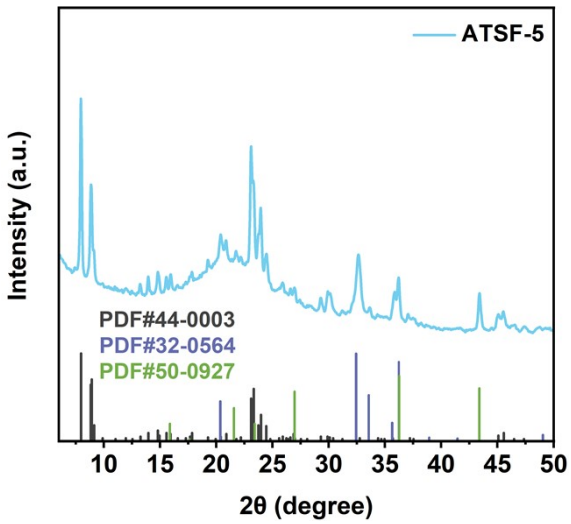

Figure S4. XRD patterns of ATSF-5 after 20 cycles.

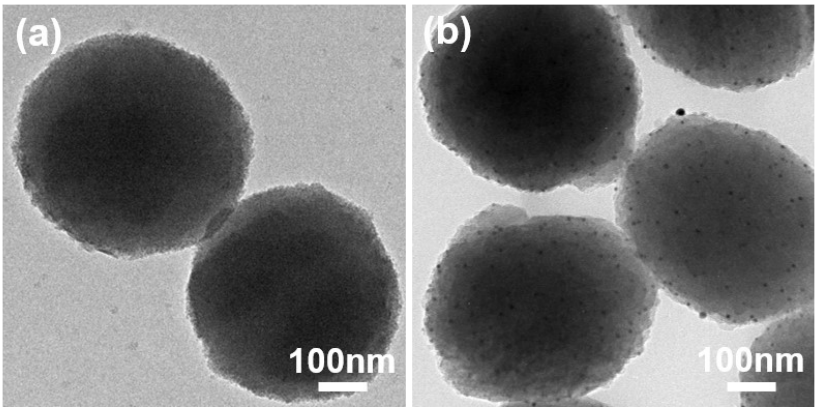

Figure S5.TEM images of (a) TS and (b) ATS.

Table S1. EDS elemental content analysis of ATS and ATSF-5.

ATS	Atomic cont. (%)	ATSF-5	Atomic cont. (%)
Ti	0.41	Ti	0.49
Si	27.91	Si	20.24
O	63.20	O	59.99
F	0.02	F	1.68
Au	0.08	Au	0.05
C	8.38	C	17.56

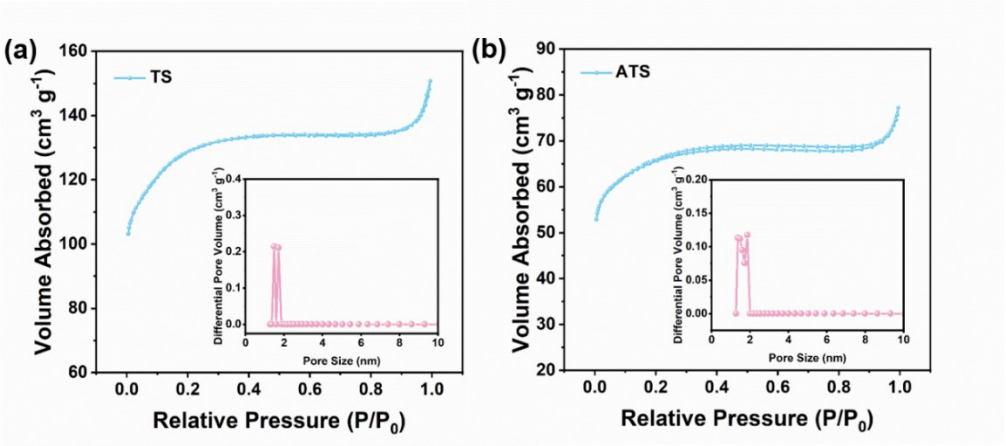

Figure S6. N_2 adsorption and desorption isothermss of (a) TS and (b) ATS-5. Inset: the distribution curves of pore sizes.

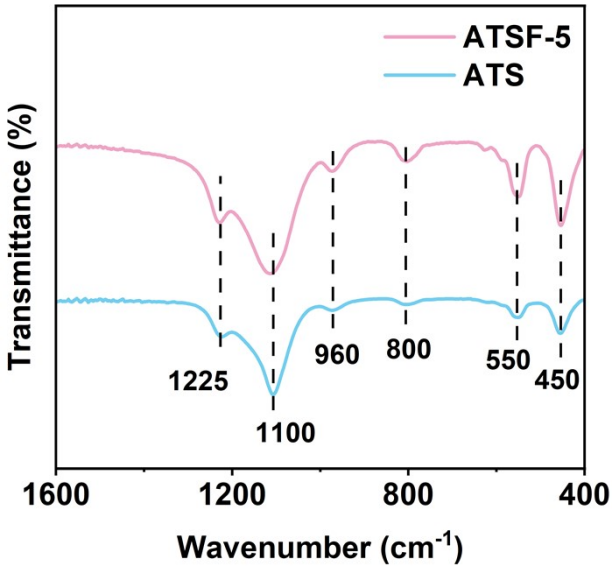

Figure S7. FTIR spectra of ATS and ATSF-5.

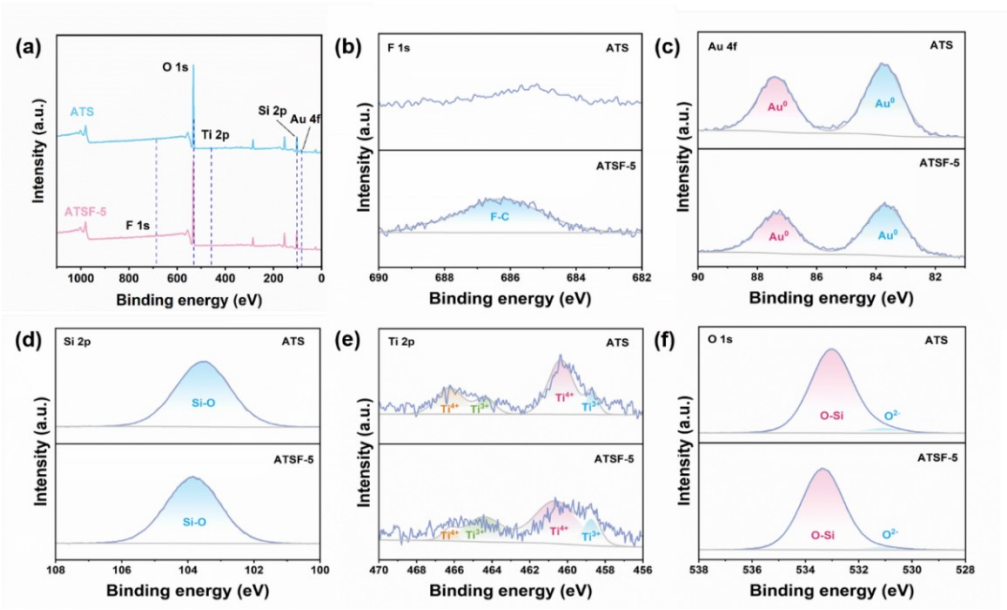

Figure S8. (a) XPS survey spectra of ATS and ATSF-5. (b-f) High-resolution XPS spectra of F 1s, Au 4f, Si 2p, Ti 2p and O 1s.

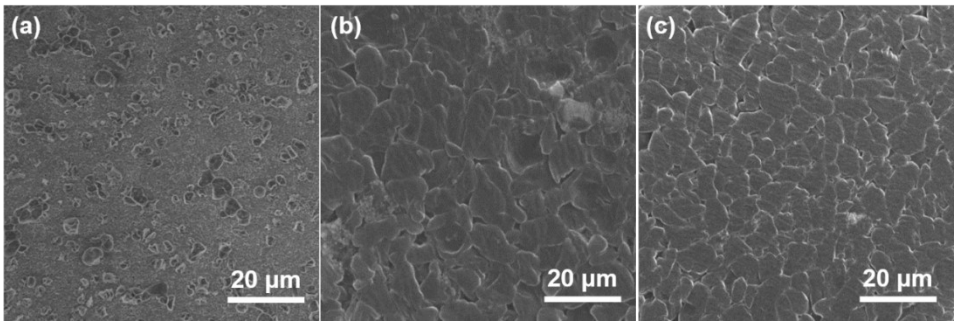

Figure S9. Top-view SEM images of the ATSF-5/Cu electrode after plating with (a) 0.2 mAh cm^{-2}, (b) 1 mAh cm^{-2} and (c) 3 mAh cm^{-2} of Li. The current density is 0.5 mA cm^{-2}.

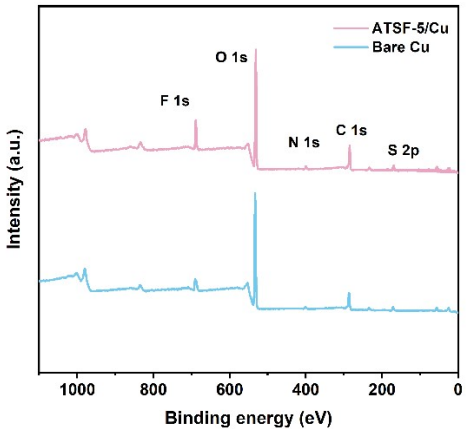

Figure S10. Survey XPS spectra of bare Cu and ATSF-5/Cu after 10 cycles.

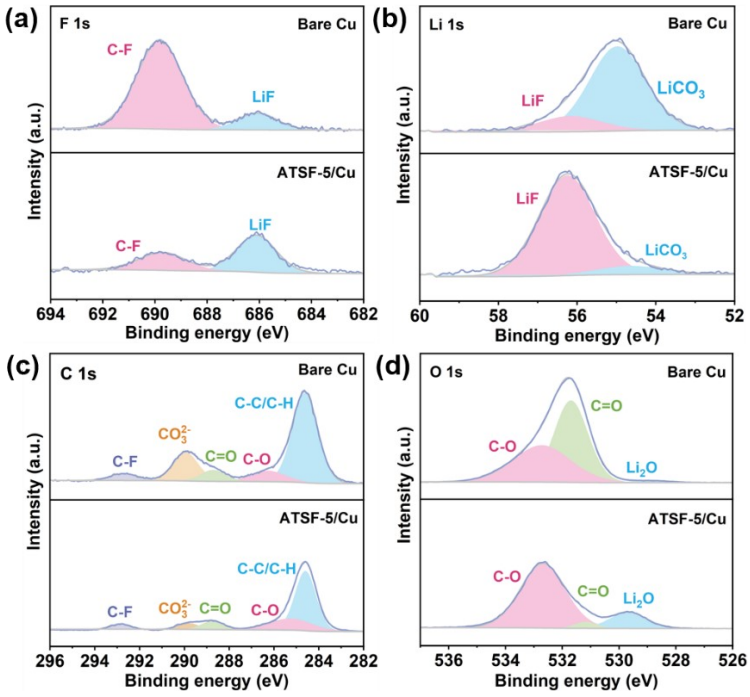

Figure S11. The XPS spectra of the bare Cu, ATSF-5/Cu after 10 cycles of (a) F 1s, (b) Li 1s, (c) C 1s and (d) O 1s.

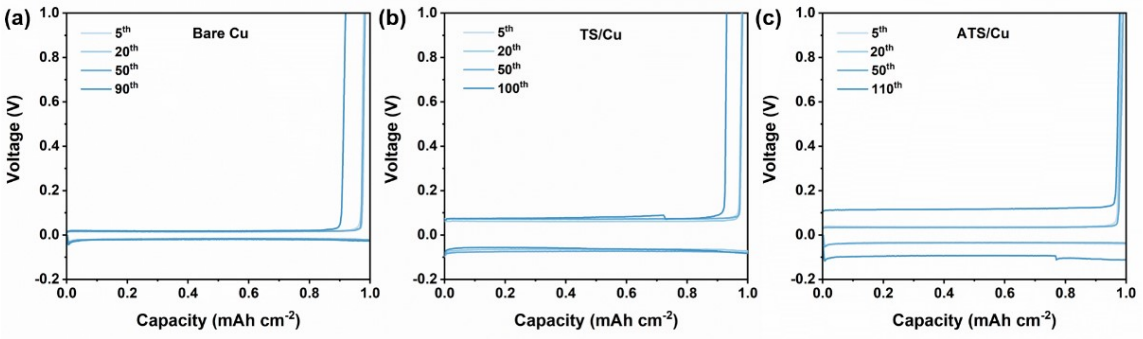

Figure S12. Voltage profiles of the Li|Cu cells with bare Cu, TS/Cu and ATS/Cu current collector at 1 mA cm^{-2} and 1 mAh cm^{-2}.

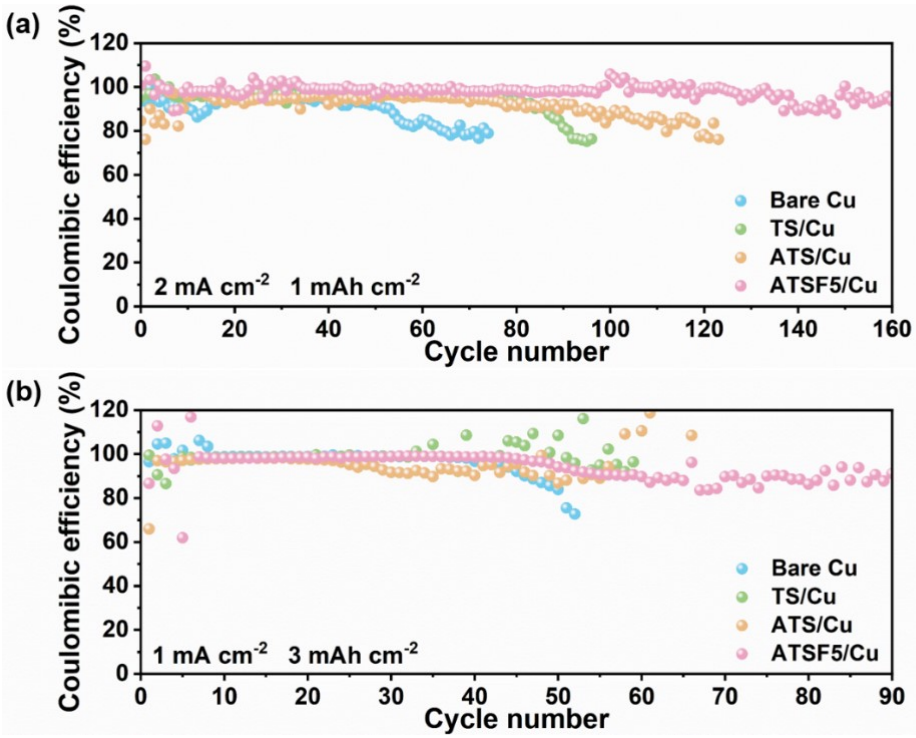

Figure S13. Comparison of CE (a) with capacity of 2 mAh·cm^{-2} at 1 mA·cm^{-2} and (b) with a capacity of 1 mAh·cm^{-2} at 3 mA·cm^{-2} of bare Cu, TS/Cu, ATS/Cu and ATSF-5/Cu electrodes.

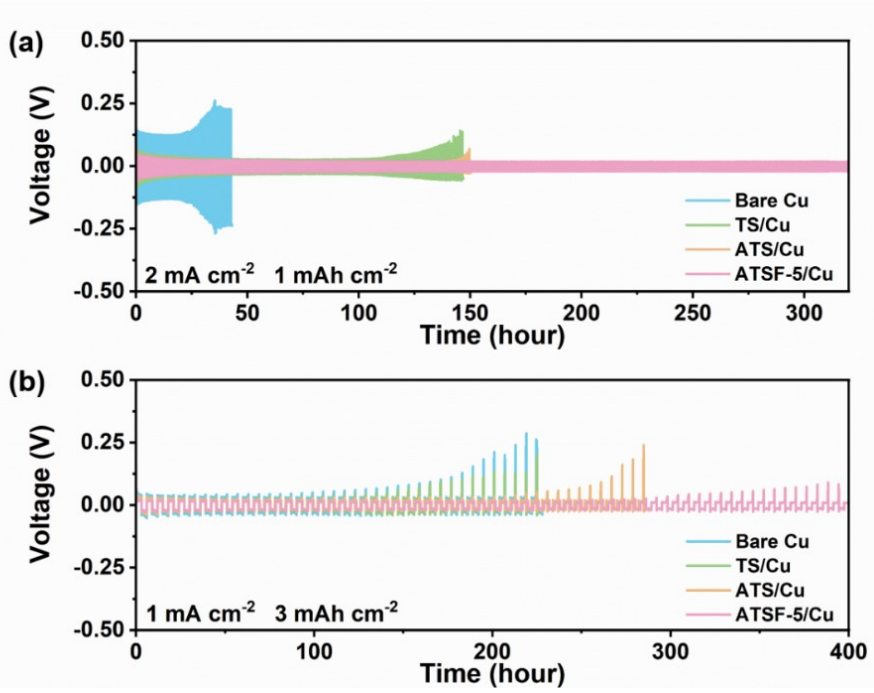

Figure S14. Voltage profiles of the symmetric cells with bare Cu, TS/Cu, ATS/Cu and ATSF-5/Cu electrodes at (a) 2 mA cm^{-2} and 1 mAh cm^{-2} and (b) 1 mA cm^{-2} and 3 mAh cm^{-2}.

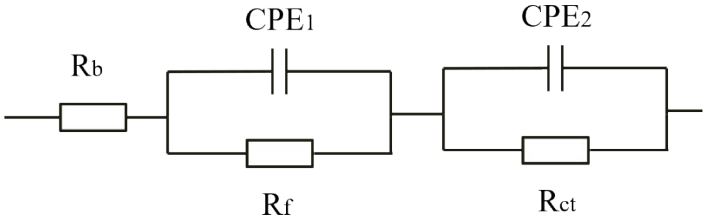

Figure S15. The equivalent circuit of the symmetric cells before and after 100 cycles, where the R_b, R_f, R_{ct} and CPE represents the ohmic impedance, SEI impedance, charge transfer impedance, and capacitance, respectively.

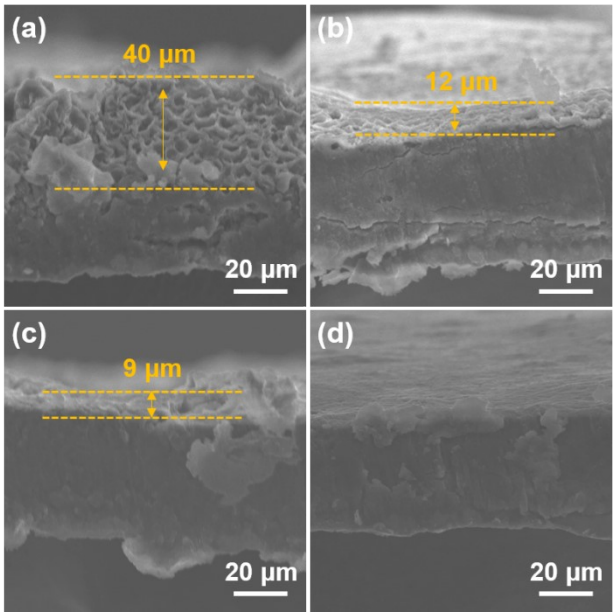

Figure S16. Cross-section SEM images of (a) bare Cu, (b) TS/Cu, (c) ATS/Cu and (d) ATSF-5/Cu electrodes disassembled from Li|Li cells after 100 cycles at 1 mA cm^{-2} and 1 mAh cm^{-2}.

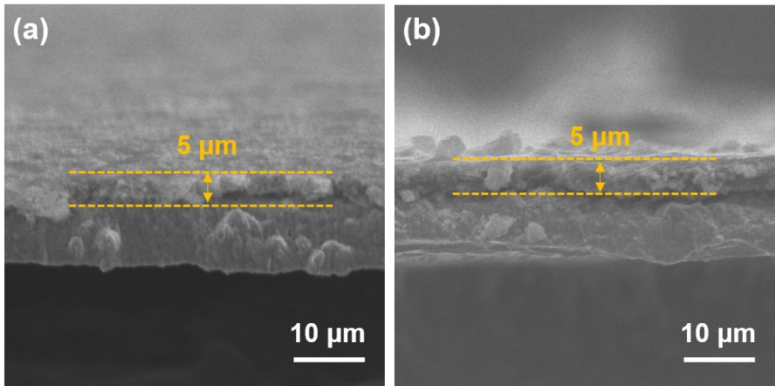

Figure S17. Cross-section SEM images of the coating layer (a) before and (b) after 100 cycles at 1 mA cm^{-2} and 1 mAh cm^{-2}.

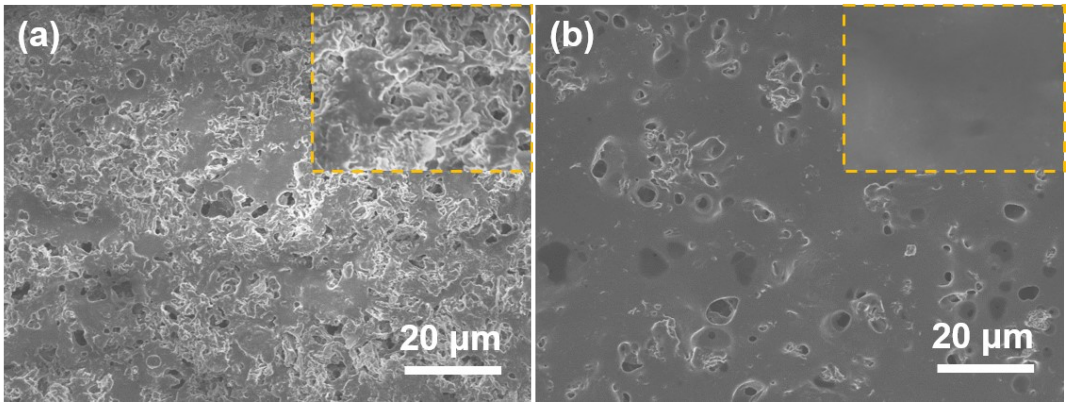

Figure S18. Ex-situ SEM images of bare Li@Cu and Li@ATSF-5/Cu electrodes disassembled from full cells after 100 cycles at 1 C.

References

S1. Kresse, G.; Furthmüller, J. Efficiency of Ab-Initio Total Energy Calculations for Metals and Semiconductors Using a Plane-Wave Basis Set. *Comput. Mater. Sci.* 1996, 6, 15−50.

S2. Kresse, G.; Furthmüller, J. Efficient Iterative Schemes for Ab Initio Total-Energy Calculations Using a Plane-Wave Basis Set. *Phys. Rev. B* 1996, 54, 11169−11186.

S3. Perdew, J. P.; Burke, K.; Ernzerhof, M. Generalized Gradient Approximation Made Simple. *Phys. Rev. Lett.* 1996, 77, 3865−3868.

S4. Kresse, G.; Joubert, D. From Ultrasoft Pseudopotentials to the Projector Augmented-Wave Method. *Phys. Rev. B* 1999, 59, 1758-1775.

S5. Blöchl, P. E. Projector Augmented-Wave Method. *Phys. Rev. B* 1994, 50, 17953-17979.

S6. S. Grimme, J. Antony, S. Ehrlich and H. Krieg, *J. Chem. Phys.*, 2010, 132, 154104.

S7. S. Grimme, S. Ehrlich and L. Goerigk, *J. Comput. Chem.*, 2011, 32, 1456-1465.